Mon. Not. R. Astron. Soc. **000**, 000–000 (0000) Printed 1 February 2008 (MN LATEX style file v2.2)

Dynamics of buoyant bubbles in clusters of galaxies

Georgi Pavlovski[1⋆], Christian R. Kaiser[1], Edward C.D. Pope[1,2,3]
[1] *School of Physics and Astronomy, University of Southampton, Southampton SO17 1BJ, U.K.*
[2] *School of Engineering Sciences, University of Southampton, Southampton SO17 1BJ, U.K.*
[3] *School of Physics and Astronomy, University of Leeds, Leeds, LS2 9JT, U.K.*

Accepted .... . Received .... ; in original form ....

ABSTRACT
We present a phenomenological model of the dynamics of buoyant bubbles in the atmosphere of a cluster of galaxies. The derived equations describe velocity, size, mass, temperature and density of the buoyant bubbles as functions of time based on several simple approximations. The constructed model is then used to interpret results of a numerical experiment of heating of the cluster core with buoyant bubbles in a hydrodynamical approximation (*i.e.* in the absence of magnetic fields, viscosity, and thermal diffusion). Based on the model parameters we discuss possible limitations of the numerical treatment of the problem, and highlight the main physical processes that govern the dynamics of bubbles in the intracluster medium.

Key words: galaxies: cooling flows – galaxies: nuclei – galaxies: active – galaxies: clusters: general – galaxies: clusters: individual: Virgo – methods: numerical

1 INTRODUCTION

Depressions of the surface brightness in X-ray images of clusters of galaxies have been identified as low density and high temperature plasma bubbles (see, *e.g.*, McNamara et al. 2000, 2001; Fabian et al. 2006), created by outflows from the central active galactic nucleus (AGN). Due to their high heat content these bubbles are thought to be one of the main heating sources of the cluster core, and the key ingredient in the solution of the cooling flow problem (Fabian 1994).

The physical process of the deposition of the heat from the bubbles into the ambient ICM is not well understood. It is partly because we do not know all the relevant physical properties of the ICM (its turbulent velocities, viscosity, *etc.*, see Schekochihin et al. (2005) for further discussion), and partly because theoretical models based on the numerical simulations with all the relevant physics are very complex, and more sophisticated numerical models, *e.g.* including realistic magnetic fields (Ruszkowski et al. 2007), are not yet very common.

In order to get a better understanding of the physical processes that determine the behaviour of AGN-blown bubbles in the ICM we start from a basic hydrodynamical model. In the present article we analyse the physics behind the results of numerical simulations of the evolution of buoyant bubbles in the atmosphere of a cluster of galaxies in the absence of magnetic fields, viscosity, and thermal diffusion. We derive equations that describe velocity, size, mass, temperature and density of the buoyant bubbles as functions of time based on several simple approximations. This approach highlights the important hydrodynamical effects, and helps to understand and discuss limitations of the numerical framework for the description of AGN bubbles. It should be viewed as a first step in the modelling process, that can isolate the phenomena caused by the simplest hydrodynamical effects.

The structure of the article is as follows: in section 2 we outline the setup of the numerical simulation, which we later use to fit our model parameters; in section 3 we describe the vortex-ring model for AGN bubbles, derive the equations that determine the evolution of the parameters of the bubbles, and determine values for the free phenomenological parameters of the model from comparison with the numerical data; in section 4 we analyse the physical properties of the model, and how numerical artifacts can affect them; in section 5 we summarise the main findings and conclusions. Appendices A, B, and C provide some background information about the hydrodynamics of the vortex rings.

2 NUMERICAL EXPERIMENT

In our previous work (Pavlovski et al. 2007, hereafter PI) we have demonstrated that the evolution of buoyant bubbles in the ICM is influenced by the hydrodynamical Kutta-Zhukovsky forces, which exist due to the circulation of the plasma in the space occupied by the bubble. One of the goals of the present work is to provide a quantitative description of the role of these forces in the overall dynamics of the bubbles.

⋆ Email: gbp@phys.soton.ac.uk (GP)

Findings in PI were based on the analysis of numerical experiments of the buoyant ascent of bubbles in the ICM. The cluster atmosphere was modelled using the observational data for the Virgo cluster (Ghizzardi et al. 2004). The bubbles were introduced *ad hoc* into an established cooling flow, at the point when the central temperature dropped below 1.5 keV. The initial temperature of the bubbles was fixed at $T = 5 \times 10^{10}$ K (a factor of 10^3 larger than the temperature of the ambient ICM). The density of the plasma inside the bubbles was calculated from the condition of the overall pressure equilibrium with the ambient medium (we tested two different pressure profiles). The initial bubbles' centres were placed symmetrically at the distance of $1.5a_0$ from the centre of the cluster, where $a_0 = 10^{22}$ cm ≈ 3.24 kpc was fixed as their initial radii, see Fig. 1. The size of the computational domain with periodic boundary conditions was 10^{24} cm. The computation was performed using the FLASH AMR hydrocode with 8 levels of refinement, resulting in a smallest cell size of $\approx 4.88 \times 10^{20}$ cm.

Our motivation for the choice of a_0 was the following. If E is the amount of energy released by an AGN, and $E_0 = fE$ is the fraction of the energy used to heat the ICM during the inflation of the bubble, then the volume of such a bubble is,

$$V_0 = E_0(\gamma - 1)/P, \tag{1}$$

where P is the ICM pressure, and $\gamma = 5/3$ is the ratio of the specific heats. For typical AGN values this gives the size of the bubble as,

$$a_0 = 3.25[\mathrm{kpc}]\left[\left(\frac{f}{0.025}\right)\left(\frac{L}{10^{42}[\mathrm{erg\,s^{-1}}]}\right)\times \left(\frac{\tau}{10^8[\mathrm{yr}]}\right)\left(\frac{10^{-3}[\mathrm{cm^{-3}}]}{n_{\mathrm{amb}}}\right)\left(\frac{10^8[\mathrm{K}]}{T_{\mathrm{amb}}}\right)\right]^{1/3} \tag{2}$$

where L is an average AGN bolometric luminosity, and τ is an average time between bubble injections, n_{amb} is the number density of the ICM, T_{amb} its temperature, and f sets the efficiency of the thermal coupling of the outflow with the ICM. We here assume f to lie in the range of a few percent (Sijacki & Springel 2006).

3 PHENOMENOLOGICAL MODEL

Analysis of the dynamics of large scale thermals and plumes in the atmosphere of the Earth (both natural and created during (nuclear) test explosions, see, *e.g.*, Turner 1957; Morton 1960; Woods 1997; Zhou et al. 2001) suggests that the evolution of hot bubbles in a stratified atmosphere can be split into two stages. Hristianovich & Rodionov (1954) proposed that during the first, relatively short stage of the ascent of a hot bubble it can be treated as remaining roughly spherical, while during the second stage its shape is best approximated by a torus. During the second stage the dynamics of the bubble is influenced by the velocity field around the bubble, which corresponds to that of a vortex ring. It is due to this velocity field that the morphology of the bubble changes (see PI for more details). Qualitative analysis of numerical simulatio of the hot bubbles in the ICM in the absence of magnetic fields done by other research groups (Gardini 2007; Reynolds et al. 2005; Brüggen & Kaiser 2002) also support this picture.

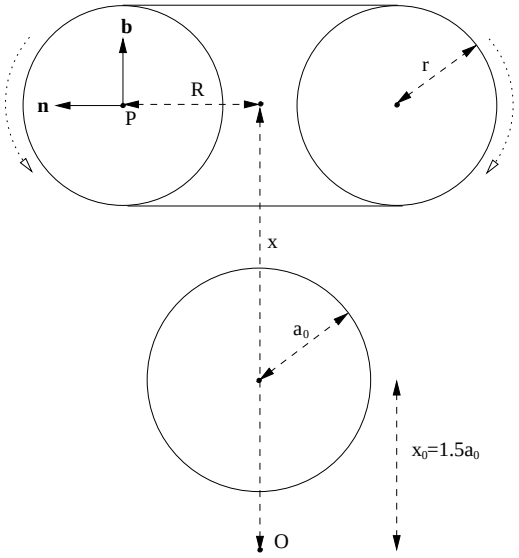

Figure 1. Initial size and position of the spherical bubble, and geometry and size of the torus-shaped bubble during the second stage of the ascent (not to scale). Point O marks the centre of the cluster, a_0 is the initial size of the bubble, $x_0 = 1.5a_0$ is its initial position. R is the radius of the torus, r is the radius of the torus cross section, P is a point on the central circle axis line of the torus, vectors **b** and **n** are accordingly the bi-normal and the normal vectors of the central circle axis line at point P (see Appendix C).

The morphological similarity of these (vastly different in size) bubbles is hardly surprising as the physical processes that govern them are very similar in the framework of a purely hydrodynamical model of the ICM and AGN bubbles. Such model is of course an oversimplification of the real phenomenon. AGN bubbles are filled with a relativistic magnetised plasma, which has an effect on the heat capacity of the plasma, and affects the diffusion properties at the bubble/ICM interface (Ruszkowski et al. 2007; Jones 2007). Here, however, we will assume that the magnetic fields are dynamically not important, and will view the plasma inside bubbles as thermal, simply having a much larger temperature.

In this rough approximation, both jet-blown ICM bubbles and buoyant thermals in the Earth's atmosphere are characterised by high temperature and density contrast, being, on average, in overall pressure equilibrium with the ambient medium. Any departure from pressure equilibrium is smoothed out on the time scale of the order of $\sim a/c$, where a is the size of the bubble, and $c = \sqrt{\gamma P/\rho}$ is the adiabatic speed of sound of the gas inside the bubble. The dynamical time scale, on the other hand, is $\sim a/c_{\mathrm{amb}}$, where c_{amb} is the adiabatic speed of sound of the ambient medium. In the case of hot, low density bubbles, $c_{\mathrm{amb}}/c \ll 1$, and we will assume that pressure equilibrium is maintained at all times. Finally, both hot bubbles in the ICM and hot atmospheric bubbles are rising due to the presence of the external gravitational field.

Based on this qualitative comparison we present a phenomenological model of the evolution of the buoyant bubbles in the ICM based on the work of Onufriev (1967) (for a recent review see Belotserkovsky et al. 2000, in Russian).

3.1 Growth of the spherical bubble

In this section we will estimate the change of the size of a spherical bubble as it ascents in a stratified atmosphere of a cluster. In a static atmosphere the only physical processes that affect the volume of the bubble are the entrainment of the colder ambient plasma (at the same pressure), change of the ambient pressure (as the bubble ascents the ambient pressure falls), and energy loss due to bremsstrahlung radiation. We can estimate the change of the volume due to these processes from the following simple argument.

Consider a hot plasma bubble ascending buoyantly a distance $\mathrm{d}x$ during the time period $\mathrm{d}t$, while a mass $\mathrm{d}M$ of the ambient gas at the temperature $T_{\rm amb}$ is entrained into it. Note, that the entrained plasma needs to be accelerated to the velocity $\mathrm{d}x/\mathrm{d}t = \dot{x}$ to travel with the bubble. However, the fraction of the total energy of the bubble which goes into the increase of the kinetic energy of the entrained plasma is going to be much smaller than the fraction of energy which goes into heating of it to the new higher temperature T, provided that the ascent speed of the bubble is smaller than the speed of sound in the ambient ICM, $|\dot{x}| < c_{\rm amb}$. Here we will ignore the kinetic energy of the entrained mass.

It is obvious that,

$$\frac{\mathrm{d}V}{V} = \frac{\mathrm{d}M}{M} - \frac{\mathrm{d}\rho}{\rho}. \tag{3}$$

To estimate the right hand side of (3) we note that in pressure equilibrium $\mathrm{d}\rho/\rho = -\mathrm{d}T/T$, and the temperature of the mixture, T, could be found from the equation of internal energy conservation,

$$T_{\rm amb}\mathrm{d}M + TM = (T + \mathrm{d}T)(M + \mathrm{d}M). \tag{4}$$

where we have ignored differences in the heat capacities of the ambient plasma and plasma inside the bubble. Hence,

$$\begin{aligned}(\zeta - 1)\frac{\mathrm{d}M}{M} &= \frac{\mathrm{d}T}{T} \\ &= -\frac{\mathrm{d}\rho_1}{\rho},\end{aligned} \tag{5}$$

where $\mathrm{d}\rho_1$ is the change of density of the bubble due to the entrainment of the mass $\mathrm{d}M$ of the ambient plasma at temperature $T_{\rm amb}$, and ζ is the *contrast parameter*,

$$\zeta = \frac{\rho}{\rho_{\rm amb}} = \frac{T_{\rm amb}}{T}, \tag{6}$$

which can be related to the X-ray detectability of the bubbles; *e.g.*, the ratio of the X-ray fluxes due to bremsstrahlung, $\propto \rho^2 T^{1/2}$, is equal to $\zeta^{3/2}$.

Using equations (6) and (3) we get the following equation for the change of volume due to the entrainment in the adiabatic homogeneous ICM,

$$\begin{aligned}\frac{\mathrm{d}V}{V} &= \zeta\frac{\mathrm{d}M}{M} \\ &= \mathrm{d}\zeta + \zeta\frac{\mathrm{d}V}{V},\end{aligned} \tag{7}$$

which has the simple solution,

$$\begin{aligned}\frac{V}{V_0} &= \frac{1-\zeta_0}{1-\zeta} \\ &= \left(\frac{a}{a_0}\right)^3,\end{aligned} \tag{8}$$

where V_0 is the initial volume of the bubble, $a_0 = 10^{22}\,\mathrm{cm} = 3.24$ kpc its initial radius and ζ_0 is the initial contrast parameter. Equation (8) is due to Hristianovich & Rodionov (1954).

In our simulations bubbles are injected with the $T_0 \approx 10^{10}$ K, and $\zeta_0 \approx 10^{-4}$. When the temperature of the bubbles falls to, *e.g.*, $T = 2\times10^7$ K, $\zeta = 0.5$, the corresponding relative change of the size of the spherical bubble (due to the entrainment) is $a/a_0 \approx 1.26$. It is worth noting that we have implicitly assumed here that the entrained material is mixed fully on time scales shorter than $|a_0/\dot{x}|$, and the bubble is homogeneous at all times. This assumption is generally not correct. The boundary layer of the bubble is entraining material, which is then getting mixed via turbulent motions or diffusion with the plasma in the bubble's centre. In this case the temperature of the bubble in not homogeneous: the temperature at the boundary of the bubble is lower then the temperature at the centre. When determining the size of the bubble from observations (or numerical data), depending on an *ad hoc* threshold in some gas property used to find the boundary of the bubble, it can appear that the bubble is getting smaller, rather then larger, as ambient ICM is entrained into it.

It is straightforward to show that the change of size of the bubble due to the change of the ambient pressure, and the loss of energy by bremsstrahlung radiation is small – generally not exceeding ten per cent.

As the bubble ascents a distance $\mathrm{d}x$, it reaches a layer with lower ambient pressure and adiabatically expands,

$$\mathrm{d}\rho_2 = \rho\frac{\mathrm{d}P}{\gamma P}. \tag{9}$$

Assuming pressure equilibrium and using equation (3) we get,

$$\frac{V}{V_0} = \left(\frac{P_0}{P}\right)^{1/\gamma}. \tag{10}$$

For a distance $x = 3.25a_0$ travelled by the bubbles in our numerical experiment (see PI), we get $a/a_0 \approx 1.12$.

The plasma inside the bubble emits bremsstrahlung radiation and cools. The density inside the bubble changes $\mathrm{d}\rho/\mathrm{d}\rho = -\mathrm{d}T/T = -\mathrm{d}E/E$, where $\mathrm{d}E$ is the loss of internal energy due to bremsstrahlung. The resulting change of the volume is,

$$\frac{V}{V_0} = 1 - \frac{\Delta E}{E}, \tag{11}$$

where ΔE is the total loss of internal energy due to bremsstrahlung during the ascent of the bubble. We can estimate the upper limit of $\Delta E/E$ using the values of density and temperature of the bubble near the end of its ascent. Using data from the numerical experiment (see PI): $\Delta t \approx 7.7\times10^{14}\,\mathrm{s}$, $\rho \approx 10^{-26}\,\mathrm{g\,cm^{-3}}$, $T \approx 10^8$ K, we get $0.99 < a/a_0 \leq 1$.

All of the mechanisms described above change the size of the bubble isotropically, and as a result the radius of the bubble towards the end of the ascent $a \approx 1.35a_0$. To account for the preferential sideways enlargement of the bubbles, eventually leading to formation of a torus, and reconcile this analysis with the numerical data, we need to consider the main forces acting on the bubble during the ascent.

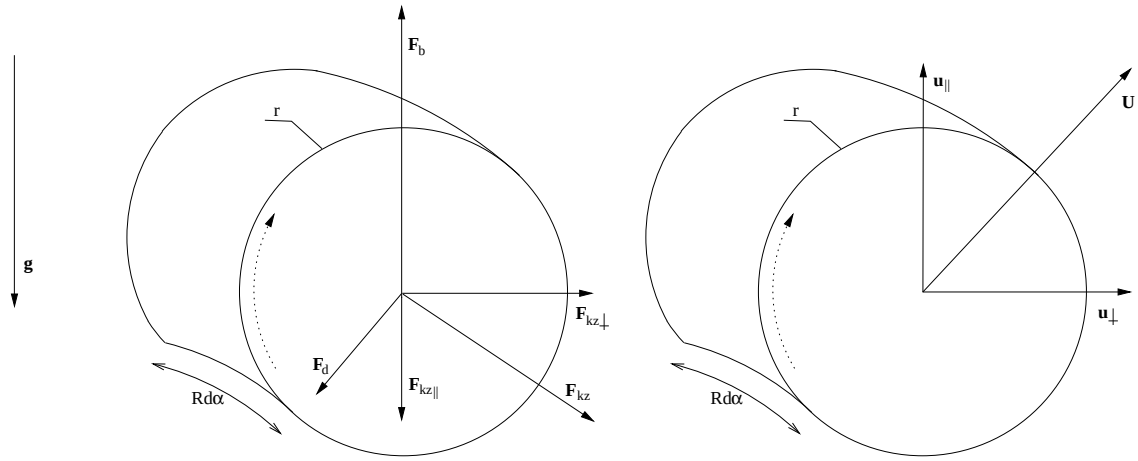

Figure 2. Right panel: forces acting on a segment (element) of the vortex ring. $F_{\rm b}$ – buoyancy, $F_{\rm d}$ – drag, $F_{\rm kz}$ – Kutta-Zhukovsky force, $F_{\rm kz||}$, $F_{\rm kz\perp}$ – components of the Kutta-Zhukovsky force. Left panel: velocity components. U – total velocity vector of the centre of mass of the vortex ring element, $u_{||}$ – vertical component of the velocity vector, $u_{\perp}$ – horizontal velocity (expansion) due to the component Kutta-Zhukovsky force $F_{\rm kz\perp}$.

3.2 Buoyant Vortex Ring

Sections 3.2, 3.3, 3.4, 3.6 are based on the work of Onufriev (1967) and Hristianovich & Rodionov (1954).

The main force that determines the ascent of the AGN blown bubbles in the ICM is created by buoyancy due to the difference in densities of plasma inside the bubbles and the ambient ICM. During the ascent the mass entrainment creates friction forces which lead to the formation of a circulational motion of gas inside the bubble and around its surface. As the speed of the ascent grows, the spherical symmetry breaks down. The initially spherical bubble expands sideways, since the pressure on the "top" and the "bottom" of the bubble becomes larger than the pressure on the sides (the velocity of the flow is larger on the sides). This process leads to the change of the shape of the bubble from spherical into torus-like, see Fig 1. Inside the torus the gas rotates around the central circle axis line, and outside the torus a circulation flow is formed.

The circulation of plasma around an element of the torus results in a Kutta-Zhukovsky force, $F_{\rm kz}$, see Fig. 2, which is perpendicular to the overall velocity, U, of the element. One of the components the Kutta-Zhukovsky force, $F_{\rm kz\perp}$, is perpendicular to the direction of the ascent ($\perp$-direction), and acts to enlarge the torus radius R. Another component of the Kutta-Zhukovsky force, $F_{\rm kz||}$, is pointing in the direction opposite to the direction of the ascent ($||$-direction) and reduces the velocity of the ascent.

The drag due to the viscosity and the kinetic energy of the wake underneath the bubble results in the drag force $F_{\rm d}$, which also acts to slow down the ascent. Note taht the $F_{\rm d}$ acts in the direction opposite U, and hence not directly opposite to $F_{\rm b}$.

3.3 Equation of motion

The rate of change of momentum of an element of the vortex ring plus the associated rate of change of momentum of the surrounding medium (the latter is modelled as the added-mass, see Appendix B) is equal to the sum of the forces acting on the vortex ring element, see Fig. 2. We can approximate the drag force using the formula applicable for a cylinder with a circular cross section of radius r moving through a fluid (Tritton 1988),

$$F_{\rm d} = \frac{1}{2} C_{\rm d} \rho_{\rm amb} U^2 \pi r^2, \tag{12}$$

where $C_{\rm d}$ is a constant, $\rho_{\rm amb}$ is the ambient density, U is the velocity of the vortex ring element, and r is the radius of its cross section. The experimental value of the constant $C_{\rm d}$ varies in range $0.1 \ldots 100$, and depends on the Reynolds number, Re, of the flow. Generally it is larger for flows with smaller Re. It is difficult to predict its value for our case, since the "cylinder" in this case is an element of the vortex ring, which is not a solid body, as it is under-dense compared to the ambient medium. The main motivation for using equation (12) is purely geometrical.

The Kutta-Zhukovsky force is proportional to the circulation, Γ, (see appendix C and PI) of the flow outside the vortex ring, and is perpendicular to the velocity, U, of the element of the torus (vortex ring),

$$F_{\rm kz} = \Gamma \rho_{\rm amb} U R {\rm d}\alpha, \tag{13}$$

where R is radius of the torus, and α is the central angle.

By projecting the vector quantities on the $||$ and $\perp$ directions, we get the following equations of motion,

$$\begin{aligned} \frac{\rm d}{{\rm d}t}\left(u_{||}\left(M+M'\right)\right) = {} & gV\rho_{\rm amb}(1-\zeta) - 2\pi\rho_{\rm amb}\Gamma R u_{\perp} \\ & - \frac{1}{2} C_{\rm d} \pi r^2 u_{||} U, \end{aligned} \tag{14}$$

and

$$\frac{\rm d}{{\rm d}t}\left(u_{\perp}\left(M+M'\right)\right) = -2\pi\rho_{\rm amb}\Gamma R u_{||} - \frac{1}{2} C_{\rm d} \pi r^2 u_{\perp} U, \tag{15}$$

where $M' = 2\pi^2 r^2 R \rho_{\rm amb}$ is the added-mass for the torus (see Appendix B), g is the gravitational acceleration, and

$$U = \sqrt{u_{\perp}^2 + u_{||}^2} \tag{16}$$

is the velocity of the torus element.

3.4 Heat balance

Entrainment of the cooler ambient plasma changes the density of the bubble according to equation (5), while the bubble also expands due to the fall of the ambient pressure as given by equation (11). From the definition of the contrast parameter,

$$\frac{\mathrm{d}\zeta}{\zeta} = \frac{\mathrm{d}\rho}{\rho} - \frac{\mathrm{d}\rho_{\rm amb}}{\rho_{\rm amb}},$$

we get the following formula for the change of contrast due to the mass entrainment and the change in the ambient pressure and density,

$$\frac{\mathrm{d}\zeta}{\zeta} = (1-\zeta)\frac{\mathrm{d}M}{M} + \frac{\mathrm{d}P}{\gamma P} - \frac{\mathrm{d}\rho_{\rm amb}}{\rho_{\rm amb}}, \tag{17}$$

which implies the following differential equation,

$$\frac{\mathrm{d}\zeta}{\mathrm{d}t} = \zeta\left[(1-\zeta)\frac{1}{M}\frac{\mathrm{d}M}{\mathrm{d}t} + \dot{x}\left(\frac{1}{\gamma P}\frac{\mathrm{d}P}{\mathrm{d}x} - \frac{1}{\rho_{\rm amb}}\frac{\mathrm{d}\rho_{\rm amb}}{\mathrm{d}x}\right)\right]. \tag{18}$$

The last term in (18), which is enclosed in round parenthesis, is a measure of the deviation of the ambient atmosphere from adiabatic conditions. For an adiabatic atmosphere $\mathrm{d}\rho_{\rm amb}/\rho_{\rm amb} = \mathrm{d}P/(P\gamma)$, and the term is exactly zero.

3.5 Mass entrainment

The entrainment of the ambient ICM into the bubble happens due to growing fluid instabilities on the surface of the bubble. The boundary layer of the buoyant bubble is corrugated by the Rayleigh-Taylor (RT) instability and becomes turbulent. The interpenetration distance h of the light fluid into the heavy fluid in a classical RT instability scenario can be written as (see, *e.g.*, Sharp 1984),

$$h = C_{\rm m} A t g t^2, \tag{19}$$

where $At = (\rho_{\rm amb} - \rho)/(\rho_{\rm amb} + \rho) = (1-\zeta)/(1+\zeta)$ is the Atwood number, g is gravitational acceleration, t is time, and $C_{\rm t}$ is a constant (see also Liu et al. 2007, for a discussion of numerical methods for mass diffusion and values of the constant). Using (19) we get the following equation for the mass transfer rate due to the RT instability,

$$\frac{1}{M}\frac{\mathrm{d}M}{\mathrm{d}t} = C_{\rm m}\frac{1-\zeta}{1+\zeta}\frac{U}{r}, \tag{20}$$

were we have substituted U for gt as it is a more appropriate measure of the velocity of the bubble/ICM interface in our case.

3.6 Size of the bubble

Using the formula for the mass of the torus,

$$M = 2\pi^2 R r^2 \rho \tag{21}$$

it is straightforward to write an equation for the change of the sizes, R and r, of the torus,

$$\frac{\mathrm{d}r}{\mathrm{d}t} = \frac{r}{2}\left[\frac{1}{M}\frac{\mathrm{d}M}{\mathrm{d}t} - \frac{1}{R}\frac{\mathrm{d}R}{\mathrm{d}t} - \frac{1}{\zeta}\frac{\mathrm{d}\zeta}{\mathrm{d}t} - \frac{\dot{x}}{\rho_{\rm amb}}\frac{\mathrm{d}\rho_{\rm amb}}{\mathrm{d}x}\right], \tag{22}$$

or, equivalently,

$$\begin{aligned}\frac{\mathrm{d}R}{\mathrm{d}t} &= u_\perp,\\ \frac{\mathrm{d}r}{\mathrm{d}t} &= \frac{r}{2}\left[\frac{1}{M}\frac{\mathrm{d}M}{\mathrm{d}t} - \frac{u_\perp}{R} - \frac{1}{\zeta}\frac{\mathrm{d}\zeta}{\mathrm{d}t} - \frac{\dot{x}}{\rho_{\rm amb}}\frac{\mathrm{d}\rho_{\rm amb}}{\mathrm{d}x}\right].\end{aligned} \tag{23}$$

3.7 Circulation

The circulation of the flow around the element of the torus is determined by the angular velocity of the fluid inside it. As the mass of the torus grows, the angular velocity of the fluid inside it decreases. Any disconnection between the inner and the outer circulation flows (*i.e.* difference in their angular velocity) leads to the production of vortices near the surface of the torus, which then are shredded away, slowing down the rotation of the flow further. It is reasonable to assume that the angular velocity is directly proportional to the circulation of the flow around the element of the torus, $\omega \propto \Gamma$. Consider a cylinder of radius r rotating in a fluid with kinematic viscosity ν around its axis of symmetry. The torque due to viscous stresses (Landau & Lifshitz 1987, §18) per unit length of this cylinder is $8\pi^2\nu\rho_{\rm amb}Rr^2\omega = 4\nu M\omega/\zeta$. The torque of the friction forces will change the angular momentum of the cylinder, $1/2Mr^2\omega$. This implies that,

$$\frac{\mathrm{d}}{\mathrm{d}t}\left(Mr^2\Gamma\right) \propto \nu M\Gamma/\zeta. \tag{24}$$

In the case of the vortex ring the role of the viscosity (friction forces) is played by the interpenetration of the fluids across the boundary of the torus. The movement of the plasma across the boundary, in other words the rate of mass entrainment, determines whether the motion of the fluid on one side of the boundary has an affect on the motion of the fluid on the other side of the boundary. Formally, from dimensional arguments we can set $\nu \propto \zeta r^2 M^{-1}\mathrm{d}M/\mathrm{d}t$. Substituting the expression for ν into equation (24) and assuming that the rate of change of the radius, $r^{-1}\mathrm{d}r/\mathrm{d}t$, is much smaller than the rate of change of the mass, $M^{-1}\mathrm{d}M/\mathrm{d}t$, we get the following equation for the change of circulation,

$$\frac{1}{\Gamma}\frac{\mathrm{d}\Gamma}{\mathrm{d}t} = -C_{\rm c}\frac{1}{M}\frac{\mathrm{d}M}{\mathrm{d}t}, \tag{25}$$

where $C_{\rm c}$ is a constant which needs to be determined from comparison with the data.

3.8 Simultaneous ODEs

The velocity of accent $\dot{x}$ is the sum of the vertical velocity of the element, $u_{||}$, which is determined by the buoyancy and the hydrodynamical forces, plus the self-induced vortex ring velocity, $v_{\rm ind}$, which is the result of the curvature $(1/R)$ of the vortex ring (see Appendix C for more information),

$$\dot{x} \equiv \frac{\mathrm{d}x}{\mathrm{d}t} = u_{||} + v_{\rm ind}, \tag{26}$$

where the induction velocity $v_{\rm ind}$ is proportional to the circulation and the curvature of the vortex ring, $\propto \Gamma/R$. In the present model we will use the expression for $v_{\rm ind}$ given by equation (C10) in Appendix C.

Together equations (26), (25), (23), (21), (20), (18), (16), (15), (14) form a closed system of ordinary differential equations (ODEs), which determines the values of eight physical parameters, $u_\perp$, $u_{||}$, R, r, x, Γ, M, and ζ as functions of time. Three phenomenological parameters, $C_{\rm d}$, $C_{\rm m}$, and $C_{\rm c}$, need to be determined by comparison with the numerical data.

3.9 Solution

The simultaneous ODEs in their dimensionless form are written in full in Appendix A. To determine the values of the phenomenological constants, $C_{\rm c,d,m}$, we have fitted the solution of the ODEs to the data from our numerical experiment C described in PI. As the initial condition we have selected a point when the bubble shape changes from spherical to toroidal. In the simulation this happens approximately 16 Myr after the injection of the bubble, and $t_0 = 722$ Myr after the start of the simulation. For reference, the dimensionless time unit is approximately 8.1 Myr, the velocity unit is $3.9 \times 10^7\,{\rm km\,s^{-1}}$, the distance unit is $10^{22}\,{\rm cm}$, and the mass unit is 9.8×10^{40} g. The initial values of the physical parameters at t_0 were measured using the averaging techniques described in PI. Their numerical values were found to be as follows, $u_\perp(t_0) = 0.26$, $u_{||}(t_0) = 0.42$, $R(t_0) = 0.99$, $r(t_0) = 0.72$, $x(t_0) = 2.56$, $\Gamma(t_0) = 2.71$, $M(t_0) = 2.4\times10^{-2}$, $\zeta(t_0) = 2.4 \times 10^{-3}$.

We solve the ODEs numerically using the adaptive step Bulirsch-Stoer method (Press et al. 2002). To find values of the phenomenological constants we minimised the function,

$$\sum_{j=1}^{42}\sum_{i=1}^{5}\frac{(X_i(t_j) - Y_i(t_j))^2}{(\Delta X_i(t_j))^2}, \qquad (27)$$

where t_j are times of the snapshots of the computational grid produced during the numerical simulation (we have 42 snapshots in total), $X_i = \{M, R, r, x, \zeta\}$ are the parameters of the bubble (torus) calculated from these snapshots, ΔX_i are their estimated errors, and $Y_i(t_j)$ are the parameters of the bubble (torus) from the solution of the simultaneous ODEs for the times t_j. The estimated errors, ΔX_i, were calculated from one sigma variations of the statistically determined quantities (see PI), and errors due to the finite grid resolution. We did not include into X_i parameters that rely on the estimation of velocities, since the comparatively large and varying time between the snapshots, $\tau(j) = t_j - t_{j-1} \neq {\rm const}$, makes it difficult to determine the values of the velocities accurately.

The best fit values for the constants were found to be $C_{\rm c} = 0.01$, $C_{\rm m} = 4$, $C_{\rm d} = 24$. Due to the uncertainties in the values of the parameters at t_0 (especially velocities and circulation) the resulting values of the constants are not determined precisely. The values of the constants are going to be different if different initial conditions are used. By varying the initial parameters by ten percent, we found that the corresponding variation of the values of the constants was approximately limited to the ranges, $C_{\rm c} \pm 0.05$, $C_{\rm m} \pm 1$, $C_{\rm d} \pm 10$.

4 ANALYSIS OF SOLUTION

In Figs. 3, 4, 5, and 6 we compare the evolution of the parameters determined from the numerical simulation, X_i, with the prediction of our model, Y_i. It is clear that the model with the best fit constants determined above, reproduces the data from the numerical experiment quite well. We achieve a good fit for the contrast parameter and the mass of the bubble over three orders of magnitude in scale. The fit for the bubble radii seems to be a bit more problematic. It is important to note, however, that by changing the initial conditions for the solution of the ODEs we can get rather better fits for radii (at least by eye). This sensitivity to the initial conditions is not surprising. We find that all Y_i, but especially radii and position, depend on the value of the initial circulation, $\Gamma(t_0)$. Since the constant $C_{\rm c} \approx 0$, the circulation remains roughly constant in time (conserved), and the precision of the measurement of the initial value is reflected in the overall quality of the fit of the parameters that depend on it directly, *i.e.* R, r, and x; the latter through the self-induced velocity of the vortex, $v_{\rm ind}$.

To illustrate the matching of the model to the three-dimensional distribution of the bubble material at different times as computed in our simulation we compare them directly in Figs. 7, 8, and 9. Note that the approximation of the bubble shape with a torus at t_0, Fig. 7, is not perfect. The distribution of the bubble material, although resembling a torus, does not have a perfectly circular cross section. The cross section of the bubble's torus is elliptical, and the size

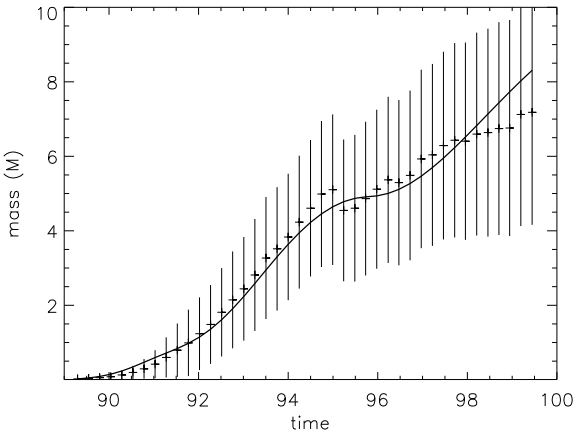

Figure 3. Growth of the bubble mass: solid line is the best fit model, points with vertical error bars are measurements from the numerical simulation.

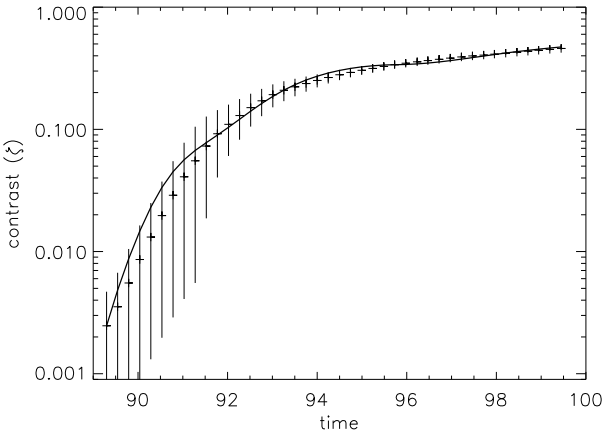

Figure 4. Change of the contrast parameter with time: solid line is the best fit model, points with error bars are measurements of the contrast paranter from the numerical simulation.

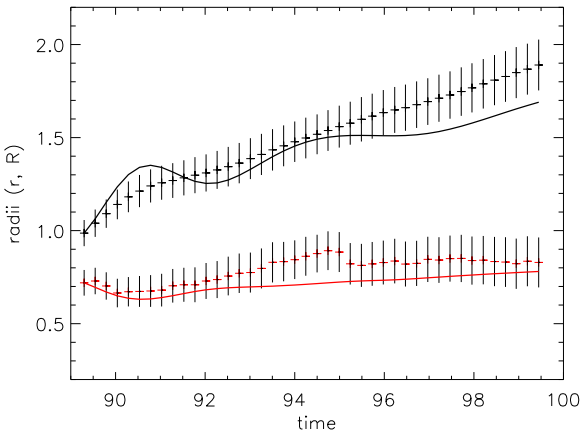

Figure 5. Growth of the bubble: solid lines are the best fit models (upper curve for R, lower curve (red) for r), dashes with the vertical error bars are measurement from the numerical simulation.

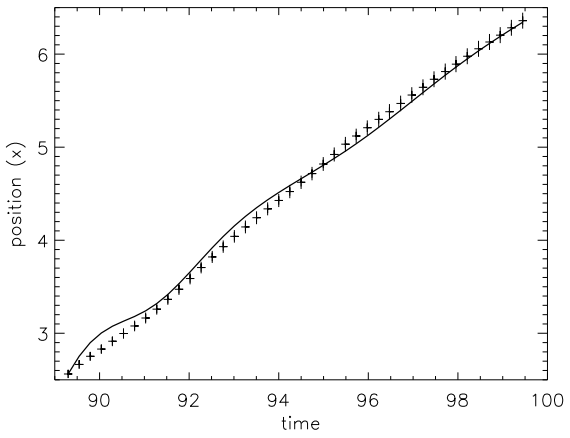

Figure 6. Ascent of the bubble: solid line – the best fit model, dashes with error bars – measurement from the numerical simulation.

of the opening at the top of the bubble is smaller than the size of the opening at the bottom of the bubble. At later times the matching of the shape of the bubble to a torus with a circular cross section is much better. Despite that, our model was able to capture the overall size and shape of the bubbles quite well.

The solution of the ODEs suggests that the vertical velocity of the bubbles due to the hydrodynamical forces, $u_{||}$, quickly falls due to significant drag, as follows from the high value of $C_\mathrm{d} \sim 30$. In fact, we find that the ascent velocity of the bubble, $\dot{x}$, in the current model is dominated by the self-induced velocity of the vortex ring, v_ind, which is an order of magnitude larger than the velocity $u_{||}$. A large drag coefficient is generally a characteristic of low Reynolds number (high viscosity) flows. Although we did not model any physical viscosity in our numerical simulation, the residual numerical viscosity is always going to be present. It is difficult to quantify its contribution. Qualitatively, however, we can state that the velocity of the ascent is more significantly affected by the the self-induced velocity of the vortex in the medium with high viscosity, and therefore large drag. In the framework of this model the bubbles will never reach "a ceiling" *i.e.* a maximum height. They will deposit their thermal content along their ascent path, but even after they reach $\zeta = 1$ and disappear the residual vortex will keep moving towards the outskirts of the cluster[1]. If the ICM has very low viscosity, the Reynolds number is likely to be much larger than a value of few hundred, which is characteristic for our present simulation. In this case the coefficient C_d can be much smaller, and $\dot{x}$ will no longer be determined by the self-induced velocity, but rather by the balance between the buoyancy and the vertical component of the Kutta-Zhukovsky force.

Another possible pitfall for our model is the overestimation of the mass diffusion across the surface of the bubble from the fit to the simulation data. It is well known (Liu et al. 2007) that generic hydro schemes tend to be super-diffusive, and yield too large values of coefficients like C_m. We can roughly estimate the impact of a possible reduction of the coefficient in the following way. By substituting equation (20) into equation (18), and neglecting the properties of the atmosphere we get,

$$\frac{\mathrm{d}\zeta}{\mathrm{d}t}\frac{1+\zeta}{\zeta(1-\zeta)^2} = C_\mathrm{m}\frac{U}{r}, \qquad (28)$$

which is easily integrable if we assume that U and r are constants,

$$\frac{2(\zeta-\zeta_0)}{(1-\zeta)(1-\zeta_0)} + \log\frac{\zeta(1-\zeta_0)}{\zeta_0(1-\zeta)} = C_\mathrm{m}\frac{U}{r}(t-t_0). \qquad (29)$$

The left hand side (l.h.s.) of equation (29) is a finite number for any given values of the contrast parameter $0 < \zeta_0 < \zeta < 1$ (l.h.s. ≈ 27 in our case: $\zeta = 0.9$, $\zeta_0 = 0.001$). Therefore, if the value of C_m is reduced by a certain factor, f, it will take f times longer for bubbles to reach the same contrast ζ. Given that the typical mass diffusion constant in simulations of RT instability is overestimated by a factor of two (Liu et al. 2007), it is quite likely that the bubbles in the ICM survive at least twice as long as a typical simulation would tend to suggest.

The small value of the constant $C_\mathrm{c} \approx 0$ implies that the circulation in our model is approximately conserved, $\Gamma \approx$ const, and the fluid is nearly ideal and incompressible. The opposite extreme $C_\mathrm{c} = 1$ corresponds to the conservation of angular momentum, $\Gamma M =$ const, see (25), and would describe a bubble unaffected by the surrounding medium.

5 DISCUSSION AND SUMMARY

The developed model is by no means a full description of the physics of buoyant bubbles in real clusters of galaxies. In this work we have tried to investigate the simplest possible approximation, and understand how different physical

[1] The drag coefficient in problem of the rise of the cloud from a nuclear explosion is much smaller, $C_\mathrm{d} \sim 0.5$. Onufriev (1967) found that in this case the cloud reaches the maximum height, which depends on the stratification of the atmosphere and its initial size.

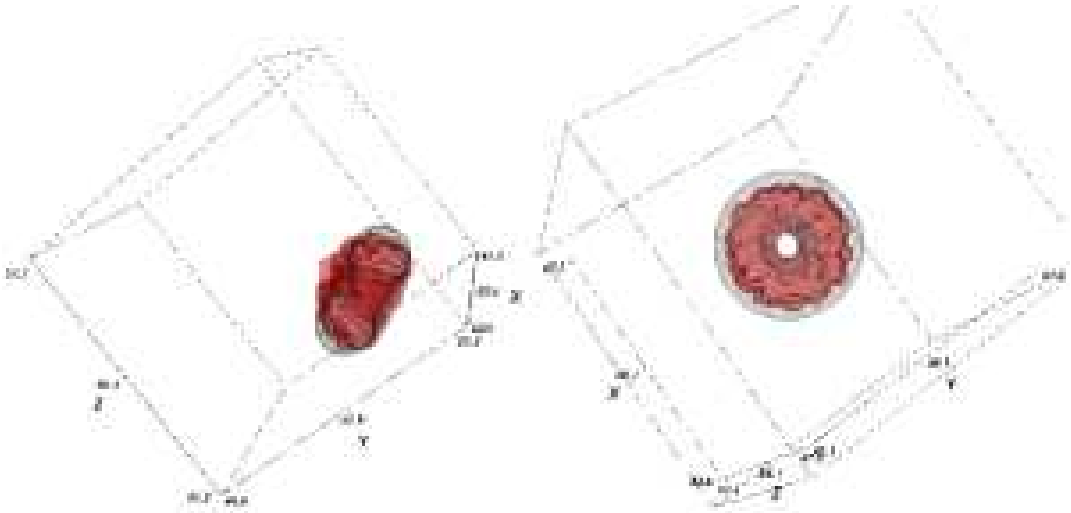

Figure 7. The initial conditions ($t = 89.1$): the distribution of the bubble material and the approximating torus.

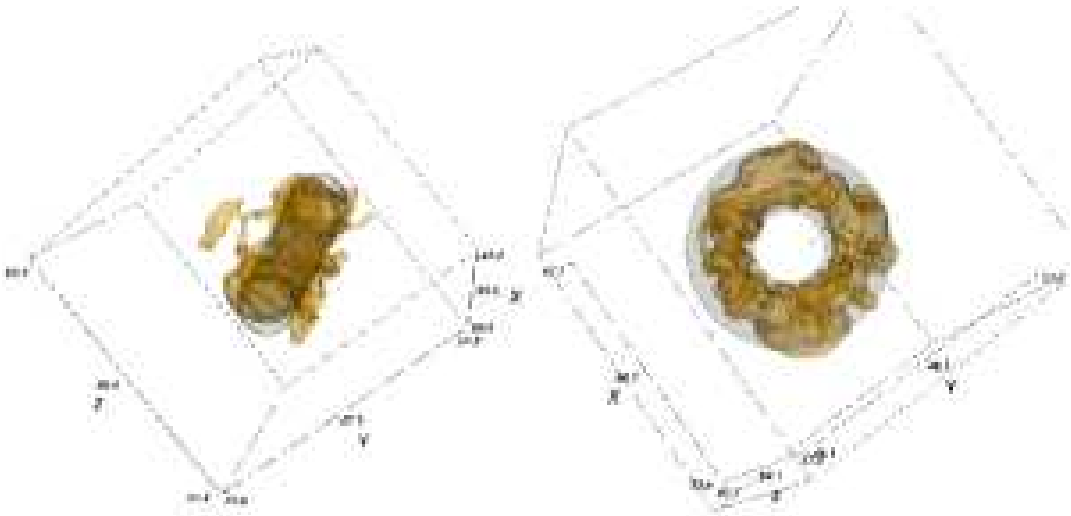

Figure 8. Comparison of the distribution of the bubble material and the approximating torus at $t = 93.9$.

properties of the bubbles are interconnected. Hydrodynamical approximations have been widely used to approximate processes of heating in clusters with AGN bubbles (*e.g.*, Brüggen & Kaiser 2002; Gardini 2007), and it is important to understand the properties of such solutions in order to know their limitations. Magnetic fields are clearly important ingredients in AGN physics. They regulate deposition of heat from the bubble into the ambient medium (Jones 2007; Ruszkowski et al. 2007) by suppressing thermal conduction around the surface of the bubble, which otherwise can lead to a rapid evaporation of the bubble (see PI).

To summarise, in this study we have developed a phenomenological model, which describes the dynamics of buoyant AGN bubbles in the atmospheres of clusters of galaxies. The value of the free phenomenological constants was determined from a comparison with the simulation data. The resulting fit of the prediction of the model to the simulation data is good. We have analysed possible outcomes that correspond to different values of the constants. The main points are as follows: 1. In low Reynolds number flows the drag coefficient is large, and the overall dynamics is determined by the circulation of the flow around the bubble. 2. Since mass entrainment is likely to be overestimated in numerical simulations, the bubbles can potentially survive in the ICM much longer than predicted by a typical simulation. 3. The conservation of circulation in our model is a consequence of the near incompressibility of the ICM (given the characteristic velocities), and absence of viscosity. Note, that the numerical viscosity alone may significantly decrease the flows Reynolds number.

The model presented here provides a framework for the interpretation of numerical and observational results. This purely hydrodynamical basis can now be extended to include more of the important physics, *e.g.* the effects of magnetic fields.

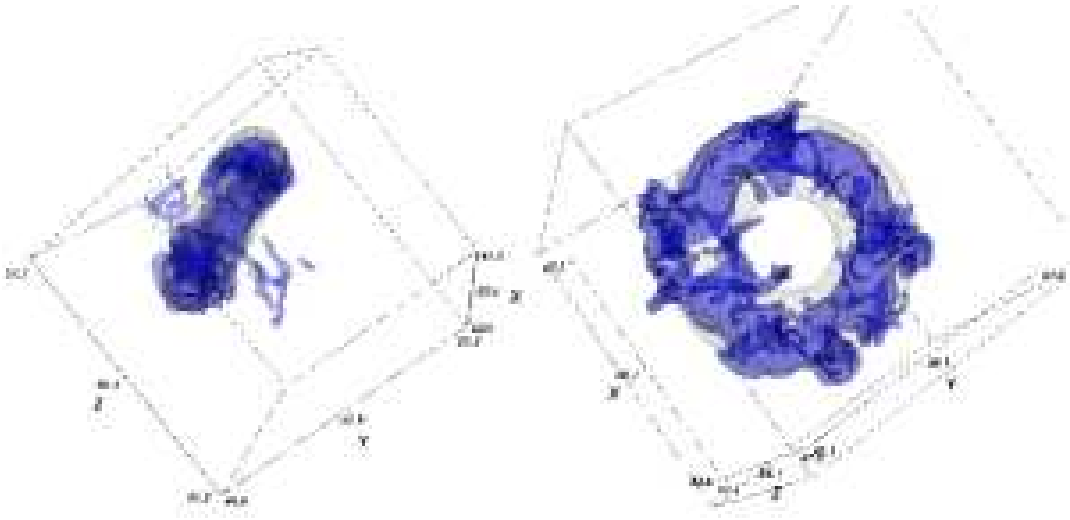

Figure 9. Comparison of the distribution of the bubble material and the approximating torus at $t = 99.4$.

6 ACKNOWLEDGEMENTS

This research has made use of NASA's Astrophysics Data System Bibliographic Services. The software used in this work was in part developed by the DOE-supported ASC / Alliance Center for Astrophysical Thermonuclear Flashes at the University of Chicago.

APPENDIX A: SYSTEM OF ODES

Equations (26), (25), (23), (21), (20), (18), (16), (15), and (14), which were derived in sections § 3.2 – 3.8 form a system of ordinary differential equations (simultaneous ODEs). The solution of these equations determines values of the bubble sideways enlargement velocity $u_\perp$, vertical velocity due to hydrodynamical forces $u_{||}$, radial size R, vertical size r, position x, circulation Γ, mass M, and contrast parameter ζ as functions of time. The identified physical processes were parametrised with the phenomenological parameters for drag C_d, mass entrainment C_m, and circulation C_c.

It is convenient to work with dimensionless variables, We since measure sizes and distances in terms of the initial size of the bubble a_0. We can use factors $\sqrt{a_0 g_0}$ for velocities and $\sqrt{a_0/g_0}$ for time to make these variables dimensionless, where g_0 is the gravitational acceleration at the starting point $g_0 = g(x_0)$. By substituting,

$$\{r, R, x\} \to \frac{\{r, R, x\}}{a_0}, \qquad \{\dot{x}, u_\perp, u_{||}\} \to \frac{\{\dot{x}, u_\perp, u_{||}\}}{\sqrt{a_0 g_0}},$$
$$t \to \frac{t}{\sqrt{a_0/g_0}}, \qquad \Gamma \to \frac{\Gamma}{a_0\sqrt{a_0 g_0}}, \tag{A1}$$

into the original equations, we get, after some simple algebra, the following ODEs describing the evolution of the parameters of the bubble: its contrast,

$$\frac{\mathrm{d}\zeta}{\mathrm{d}t} = \zeta\left[(1-\zeta)\frac{1}{M}\frac{\mathrm{d}M}{\mathrm{d}t} + \dot{x}\frac{\mathrm{d}}{\mathrm{d}x}\log(P^{1/\gamma}\rho_\mathrm{amb}^{-1})\right], \tag{A2}$$

its sizes,

$$\frac{\mathrm{d}r}{\mathrm{d}t} = \frac{r}{2}\left[\frac{1}{M}\frac{\mathrm{d}M}{\mathrm{d}t} - \frac{u_\perp}{R} - \frac{1}{\zeta}\frac{\mathrm{d}\zeta}{\mathrm{d}t} - \dot{x}\frac{\mathrm{d}}{\mathrm{d}x}\log\rho_\mathrm{amb}\right],$$
$$\frac{\mathrm{d}R}{\mathrm{d}t} = u_\perp, \tag{A3}$$

its characteristic velocities,

$$\frac{\mathrm{d}u_{||}}{\mathrm{d}t} = \frac{1-\zeta}{1+\zeta}g - \frac{\Gamma u_\perp}{\pi(1+\zeta)r^2} + u_{||}\left[\frac{1}{\zeta(1+\zeta)}\frac{\mathrm{d}\zeta}{\mathrm{d}t} - \frac{1}{M}\frac{\mathrm{d}M}{\mathrm{d}t} - \frac{C_\mathrm{d}}{4\pi}\frac{U}{R(1+\zeta)}\right],$$
$$\frac{\mathrm{d}u_\perp}{\mathrm{d}t} = \frac{\Gamma u_{||}}{\pi(1+\zeta)r^2} + u_\perp\left[\frac{1}{\zeta(1+\zeta)}\frac{\mathrm{d}\zeta}{\mathrm{d}t} - \frac{1}{M}\frac{\mathrm{d}M}{\mathrm{d}t} - \frac{C_\mathrm{d}}{4\pi}\frac{U}{R(1+\zeta)}\right], \tag{A4}$$
$$U = \sqrt{u_\perp^2 + u_{||}^2},$$

its position (height),

$$\dot{x} = u_{||} + v_\mathrm{ind},$$
$$v_\mathrm{ind} = \frac{\Gamma}{4\pi R}\left[\log\frac{8R}{r} - \frac{1}{4} - \frac{12\log(8R/r) - 15}{32}\left(\frac{r}{R}\right)^2\right], \tag{A5}$$

circulation of the ICM around it,

$$\frac{\mathrm{d}\Gamma}{\mathrm{d}t} = -C_\mathrm{c}\frac{\Gamma}{M}\frac{\mathrm{d}M}{\mathrm{d}t}, \tag{A6}$$

and the mass entrainment rate,

$$\frac{\mathrm{d}M}{\mathrm{d}t} = C_\mathrm{m}\frac{1-\zeta}{1+\zeta}\frac{UM}{r}. \tag{A7}$$

APPENDIX B: ADDED-MASS

A body moving through a continuous medium creates a velocity field in that medium. A spherical bubble ascending in a static atmoshpere of a cluster of galaxies creates a velocity

field in the cluster. The total kinetic energy of the system, which consists of the moving bubble plus the ambient atmosphere, is the sum of the kinetic energy of the of the medium (the kinetic energy of the induced velocity field), plus the kinetic energy of the bubble. It is possible to show that such motion can be described as a motion of a spherical bubble with an effective mass, which consists of its own mass plus an added-mass, which is proportional to the mass of the medium displaced by the body. Here we will assume that the flow is laminar, potential (*i.e.* non-rotational), and the bubble has a constant radius.

The velocity field in an ideal incompressible fluid with zero vorticity can be described by the equation,

$$\nabla \times \mathbf{v} = 0, \tag{B1}$$

or equivalently,

$$\mathbf{v} = -\nabla\psi. \tag{B2}$$

Using the incompressibility ($\nabla \cdot \mathbf{v} = 0$) condition we get,

$$\nabla^2\psi = 0, \tag{B3}$$

which is the well-known Laplace equation for the velocity potential, ψ.

Consider a uniform flow of an incompressible, non-rotational fluid past a sphere. By uniform flow here we mean that at large distances from the sphere the flow has a uniform velocity $U\mathbf{k}$, where $\mathbf{k}$ is the unit vector (along the z axis) of a Cartesian coordinate system. We can chose the centre of the sphere as the centre for the coordinate system. If the radius of the sphere is a, then we have to solve the Laplace equation (B3) in the region $a \le r \le \infty$. The boundary condition applied to the surface of the sphere is,

$$\left(\frac{\partial\psi}{\partial r}\right)_{r=a} = 0. \tag{B4}$$

The boundary condition at infinity can be taken to be,

$$\psi = -Ur\cos\theta, \quad \text{at} \quad r \to \infty, \tag{B5}$$

which would give the velocity (in a spherical system of coordinates),

$$\mathbf{v}(r,\theta,\phi) = U\cos\theta\mathbf{e}_r - U\sin\theta\mathbf{e}_\theta, \quad \text{when } r \to \infty, \tag{B6}$$

where we used the relation $\mathbf{k} = \cos\theta\mathbf{e}_r - \sin\theta\mathbf{e}_\theta$.

The general solution of the Laplace equation (B3) in spherical coordinates is,

$$\begin{aligned}\psi =& \sum_{l=0}^{\infty}\sum_{m=0}^{l}\left(A_l r^l + B_l r^{-l-1}\right)P_l^m(\cos\theta)\times \\ &\times\left[S_l^m\sin\phi m + C_l^m\cos\phi m\right],\end{aligned} \tag{B7}$$

where P_l^m are the associated Legendre functions (Morse & Feshbach 1953).

The boundary conditions (B4) and (B5) can be satisfied only for the following combination,

$$\psi = -U\left(r + \frac{a^3}{2r^2}\right)\cos\theta. \tag{B8}$$

The velocity of the flow can be easily found using (B2),

$$\mathbf{v} = U\mathbf{k} - U\frac{a^3}{r^3}\left(\cos\theta\mathbf{e}_r - \frac{1}{2}\sin\theta\mathbf{e}_\theta\right). \tag{B9}$$

With a simple Galilean transformation we can now consider the problem of motion of the sphere with velocity $U\mathbf{k}$ through a fluid at rest (at infinity). If we take the origin of the new coordinate system at the instantaneous position of the centre of the sphere, then the flow pattern around the sphere is given by,

$$\mathbf{v}' = -U\frac{a^3}{r^3}\left(\cos\theta\mathbf{e}_r - \frac{1}{2}\sin\theta\mathbf{e}_\theta\right). \tag{B10}$$

The kinetic energy of the fluid around the sphere is,

$$\begin{aligned}K_{\text{fluid}} =& \frac{1}{2}\rho\int_0^{2\pi}\int_0^{\pi}\int_a^{\infty}\mathbf{v}'^2 r^2\sin\theta\mathrm{d}r\mathrm{d}\theta\mathrm{d}\phi \\ =& \frac{1}{3}\pi\rho a^3U^2 \\ =& \frac{1}{2}M'U^2,\end{aligned} \tag{B11}$$

where $M' = 1/2V\rho$, $V = 4/3\pi a^3$. The total kinetic energy of the system fluid plus the sphere is equal to the sum of the kinetic energy of the sphere and the kinetic energy of the fluid,

$$K = \frac{1}{2}\left(M + M'\right)U^2, \tag{B12}$$

and can be interpreted as the kinetic energy of the sphere with the *effective mass* of $M + M'$ – the mass of the sphere plus an added-mass equal to half of the displaced mass of the fluid.

A similar derivation for a cylinder yields (see *e.g.*, Choudhuri 1998) $M' = V\rho$, where V is the volume of the cylinder. If we consider an element of the vortex ring to be roughly cylindrical, then for a whole torus moving in the || direction, the added-mass also should be equal to the total mass of the displaced fluid, $M' = V\rho$, where $V = 2\pi^2r^2R$ is the volume of a torus. A rigorous mathematical treatment of the problem (Miloh et al. 1978) proves this approximation to be accurate to within a few per cent, $1 \le M'/(V\rho) < 1.0625$.

Note that the motion of *two* identical spheres in opposite directions along a line connecting their centres with velocities $U = U_1 = -U_2$, yields the expression for the kinetic energy of the fluid (Lamb 1932),

$$2K = \rho V\left(1 - \frac{3}{16}\frac{a^3}{x^3} + O\left(\frac{a^6}{x^6}\right)\right)U^2, \tag{B13}$$

where $V = 4/3\pi a^3$ is the volume of the sphere, and x is half of the distance between the spheres. Equation (B13) implies that the resulting effective mass for a sphere in the presence of an identical sphere moving in the opposite direction is slightly lower than that of a single sphere. Therefore, our approximation of the added-mass of the torus, $M' = V\rho$, which is slightly lower than the value for a single torus as given by calculations of Miloh et al. (1978) is, in fact, appropriate since in our cluster there are two bubbles, *i.e.* there is a second torus, which is moving with the same speed in the opposite direction.

APPENDIX C: VELOCITY INDUCED BY THE VORTEX RING

The motion of the gas in cluster around the toroidal bubble is not irrotational. While the results of the previous section

remain valid, they are incomplete. To describe motion of the gas around a toroidal bubble we have to take into account the rotation of the gas around the centre line of the torus. The rotation itself does not change the value of the added-mass, but it is essential for proper treatment of the velocity field around the toroidal bubble.

The following general discussion is based on the material from Batchelor (1967).

Consider an incompressible fluid with the velocity field, $\mathbf{v}$,

$$\nabla \cdot \mathbf{v} = 0,$$

which can be described in terms of the vector potential, $\mathbf{B}$,

$$\mathbf{v} = \nabla \times \mathbf{B}, \tag{C1}$$

and vorticity vector $\boldsymbol{\omega}$,

$$\boldsymbol{\omega} = \nabla \times \mathbf{v}.$$

The above equations imply

$$\nabla (\nabla \cdot \mathbf{B}) - \nabla^2 \mathbf{B} = \boldsymbol{\omega}. \tag{C2}$$

Se can seek a solution of (C2) in the volume where $\nabla \cdot \mathbf{B} = 0$, so that,

$$\nabla^2 \mathbf{B} = -\boldsymbol{\omega},$$

and

$$\mathbf{B}(\mathbf{x}) = \frac{1}{4\pi} \int \frac{\boldsymbol{\omega}(\mathbf{x}')}{s} \mathrm{d}V(\mathbf{x}'), \tag{C3}$$

where $s = |\mathbf{x} - \mathbf{x}'|$. Using (C3) the gauge $\nabla \cdot \mathbf{B} = 0$ reduces to $\boldsymbol{\omega} \cdot \mathbf{n} = 0$, where $\mathbf{n}$ is the normal vector to the boundary of the fluid. The latter can always be satisfied in a volume possibly extended beyond the physical boundary (Batchelor 1967, §2.4). Using (C1) we find the velocity of the fluid in terms of the vorticity vector,

$$\mathbf{v}(\mathbf{x}) = -\frac{1}{4\pi} \int \frac{\mathbf{s} \times \boldsymbol{\omega}(\mathbf{x}')}{s^3} \mathrm{d}V(\mathbf{x}'). \tag{C4}$$

The *vortex-line* (by analogy with the flow line) is the line whose tangent vector is everywhere parallel to the local value of the vorticity $\boldsymbol{\omega}$. The *vortex-tube* is a surface constructed by all vortex lines passing through a given reducible closed curve C[2]. The integral of vorticity over an open surface A bounded by the same closed curve C, lying on a vortex tube and passing round it once is independent of the choice of the line and, therefore, the surface A. In other words, the flux of vorticity through the vorticity-tube, along the vortex-line, is conserved. The value of the surface integral over the surface A, i.e. the flux of vorticity through a cross section of the vortex-tube, is called the strength of the vortex tube,

$$\Gamma = \int_A \boldsymbol{\omega} \cdot \mathbf{n} \mathrm{d}A = \oint_C \mathbf{v} \cdot \mathrm{d}x.$$

The line integral is taken over a closed line, C, lying on the vortex-tube and passing around it once. It is called *circulation*.

[2] This definition of the vortex-tube is identical to the definition of the flux tubes in a magnetic field. Further analogies do also hold, *e.g.*, (C6) is analogues to the Biot–Savart law, where the line vortex plays the role of a current, and velocity plays the role of the resulting magnetic field.

The *line vortex* is a useful mathematical abstraction in cases when the vorticity is large in a limited volume (in the vicinity of a line) and negligible elsewhere. If $\delta\mathbf{l}$ is a vector element of the line vortex which lies in the volume δV, by the definition we have,

$$\int_{\delta V} \boldsymbol{\omega} \mathrm{d}V = \Gamma \delta \mathbf{l}, \tag{C5}$$

where Γ is the strength of the vortex tube constructed around the line vortex. Using (C5) and (C4) it is straightforward to get the velocity distribution of the fluid,

$$\mathbf{v}(\mathbf{x}) = -\frac{\Gamma}{4\pi} \oint \frac{\mathbf{s} \times \mathrm{d}\mathbf{l}(\mathbf{x}')}{s^3}, \tag{C6}$$

where $\mathbf{s}$ is the vector connecting the point $\mathbf{x}$ in the flow with the point $\mathbf{x}'$ on the line vortex.

C1 Application to buoyant bubbles

We have argued (PI) that the velocity field of plasma induced by the ascending bubbles is that of a vortex ring, *i.e.* a circular line vortex of radius R and strength Γ. Using (C6) it is easy to get an expression of the velocity of the plasma directly under the rising circular line vortex (vortex ring),

$$v(x) = \frac{\Gamma R^2}{2(x^2 + R^2)^{3/2}}, \tag{C7}$$

where x is the distance from the centre of the bubble to the point directly under it. This is the velocity with which the material will be lifted up from the centre of the cluster by the ascending bubble due to the circulation.

The velocity field induced by the vortex ring has another interesting property. It is obvious from (C6) that there is a singularity in the velocity field at the points on the vortex. Careful examination of the velocity field in the vicinity of the line vortex (Batchelor 1967) shows that the velocity field near the vortex consists of the rotational motion around it plus a translational motion. If $\mathbf{t}$, $\mathbf{n}$, $\mathbf{b}$ are the tangent, the normal, and the binormal vectors of the line vortex at the point P, then the position of a point in the plane perpendicular to the line vortex at P can be written as,

$$\mathbf{r} = q_2 \mathbf{n} + q_3 \mathbf{b}.$$

The velocity field at the distance $r = \sqrt{q_2^2 + q_3^2} \to 0$ near the point P, see Fig. 1, has the asymptotics (Batchelor 1967, § 7.1),

$$\frac{\Gamma}{2\pi r} (\mathbf{b} \cos\phi - \mathbf{n} \sin\phi) + \frac{\Gamma}{4\pi R} \mathbf{b} \log \frac{R}{r} + O\left(r^0\right), \tag{C8}$$

where ϕ is a polar angle in the plane defined by the vectors $\mathbf{n}$ and $\mathbf{b}$. The first term in (C8) represents the expected circulatory motion about the line vortex. The second term shows that there is another weaker singularity of the velocity distribution associated with the local curvature of the line vortex, this is the induced velocity,

$$\mathbf{v}_{\mathrm{ind}} = \mathbf{b} v_{\mathrm{ind}},$$
$$v_{\mathrm{ind}} = \frac{\Gamma}{4\pi R} \mathbf{b} \log \frac{R}{r} + O\left(r^0\right).$$

The velocity of the fluid in the vicinity of point P has a large velocity in the direction of the binormal, with a magnitude varying asymptotically as $\log 1/r$.

Lamb (1932) (Ch. 7) gives a proof of the Kelvin formula for the self induced velocity of a circular vortex ring of a small cross section in a perfect fluid,

$$v_{\rm ind} = \frac{\Gamma}{4\pi R}\left[\log\frac{8R}{r} - \frac{1}{4} + o\left(\frac{r}{R}\right)\right]. \qquad \text{(C9)}$$

In case when the vorticity is confined to the surface of the ring (so called hollow vortex), the term $-1/4$ is replaced by $-1/2$ (Hicks 1883).

Equation (C9) was applied to buoyant vortex rings by Turner (1957) (see also Morton 1960; Turner 1969; Woods 1997). The general problem was re-examined by Fraenkel (1972), who proved the existence of steady vortex rings, and gave a generalisation of (C9) for arbitrary distributions of vorticity as a function of r, and Saffman (1970) for the case of viscous vortex rings. Onufriev (1967) used the following formula for the induced velocity for description of motion of the cloud from a nuclear explosion,

$$v_{\rm ind} \approx \frac{\Gamma}{4\pi R}\left[\log\frac{8R}{r} - \frac{1}{4} - \frac{12\log(8R/r) - 15}{32}\left(\frac{r}{R}\right)^2\right]. \qquad \text{(C10)}$$

REFERENCES

Batchelor G. K., 1967, An introduction to fluid dynamics. Cambridge University Press

Belotserkovsky O. M., Andruschenko V. A., Shevelev Y. D., 2000, Dynamics of spacial and vortex flows in the inhomogeneous atmosphere: A numerical experiment. Moscow: Yanus-K

Brüggen M., Kaiser C. R., 2002, Nat., 418, 301

Choudhuri A. R., 1998, The Physics of Fluids and Plasmas. Cambridge University Press

Fabian A. C., 1994, ARA&A, 32, 277

Fabian A. C., Sanders J. S., Taylor G. B., Allen S. W., Crawford C. S., Johnstone R. M., Iwasawa K., 2006, MNRAS, 366, 417

Fraenkel L. E., 1972, J. Fluid Mech., 51, 119

Gardini A., 2007, A&A, 464, 143

Ghizzardi S., Molendi S., Pizzolato F., De Grandi S., 2004, ApJ, 609, 638

Hicks W. M., 1883, Royal Society of London Proceedings Series I, 35, 304

Hristianovich S. A., Rodionov V. N., 1954, Technical report, On the rise of a cloud. Inst. Chem. Phys. Ac. Sci. USSR

Jones T. W., 2007, ArXiv e-prints, 708

Lamb H., 1932, Hydrodynamics. Cambridge University Press

Landau L. D., Lifshitz E. M., 1987, Fluid Mechanics, second edn. Vol. 4, Pergamon Press

Liu X., Li Y., Glimm J., Li X. L., 2007, Journal of Computational Physics, 222, 644

McNamara B. R., Wise M., Nulsen P. E. J., David L. P., Sarazin C. L., Bautz M., Markevitch M., Vikhlinin A., Forman W. R., Jones C., Harris D. E., 2000, ApJ, 534, L135

McNamara B. R., Wise M. W., Nulsen P. E. J., David L. P., Carilli C. L., Sarazin C. L., O'Dea C. P., Houck J., Donahue M., Baum S., Voit M., O'Connell R. W., Koekemoer A., 2001, ApJ, 562, L149

Miloh T., Waismann G., Weihs D., 1978, Jour. of Eng. Math., 12, 1

Morse P. M., Feshbach H., 1953, Methods of Theoretical Physics, Part II.. New York: McGraw-Hill

Morton B. R., 1960, J. Fluid Mech., 9, 107

Onufriev A. T., 1967, Jour. of Appl. Mech. and Thech. Phys., 8, 3

Pavlovski G., Kaiser C. R., Pope E. C. D., Fangohr H., 2007, Morphology of flows and buoyant bubbles in the Virgo cluster, submitted, arXiv:0709.1790

Press W. H., Teukolsky S. A., Vetterling W. A., Flannery B. P., 2002, Numerical Recipes in C++. The art of scientific computing, second edn. Vol. Volume 1 of Fortran Numerical Recipes, Cambridge University Press

Reynolds C. S., McKernan B., Fabian A. C., Stone J. M., Vernaleo J. C., 2005, MNRAS, 357, 242

Ruszkowski M., Enßlin T. A., Brüggen M., Heinz S., Pfrommer C., 2007, MNRAS, pp 400–+

Saffman P. G., 1970, Stud. Appl. Math., 49, 371

Schekochihin A. A., Cowley S. C., Kulsrud R. M., Hammett G. W., Sharma P., 2005, in 'The Magnetized Plasma in Galaxy Evolution' Krakow, Poland, Sept. 27th - Oct. 1st, 2004 Magnetised plasma turbulence in clusters of galaxies. p. 200

Sharp D. H., 1984, Physica D Nonlinear Phenomena, 12, 3

Sijacki D., Springel V., 2006, MNRAS, 366, 397

Tritton D. J., 1988, Physical Fluid Dynamics, 2nd ed. edn. Oxford, England: Oxford University Press

Turner J. S., 1957, Proc. Roy. Soc. A., 239, 61

Turner J. S., 1969, Annu. Rev. Fluid Mech., 1, 29

Woods A. W., 1997, J. Fluid. Mech., 345, 347

Zhou X., Luo K. H., Williams J. J. R., 2001, Eur. J. Mech. B. - Fluids, 20, 233